

# Optimizing HVOF Spray Parameters to Maximize Bonding Strength of WC-CrC-Ni Coatings on AISI 304L Stainless Steel

C. Thiruvikraman, V. Balasubramanian, and K. Sridhar

(Submitted December 18, 2013; in revised form February 21, 2014)

High velocity oxygen fuel (HVOF)-sprayed cermet coatings are extensively used to combat erosion-corrosion in naval applications and in slurry environments. HVOF spray parameters such as oxygen flow rate, fuel flow rate, powder feed rate, carrier gas flow rate, and spray distance have significant influence on coating characteristics like adhesion bond strength and shear strength. This paper presents the use of statistical techniques in particular response surface methodology (RSM), analysis of variance, and regression analysis to develop empirical relationships to predict adhesion bond strength and lap shear bond strength of HVOF-sprayed WC-CrC-Ni coatings. The developed empirical relationships can be effectively used to predict adhesion bond strength and lap shear bond strength of HVOF-sprayed WC-CrC-Ni coatings at 95% confidence level. Response graphs and contour plots were constructed to identify the optimum HVOF spray parameters to attain maximum bond strength in WC-CrC-Ni coatings.

**Keywords** bond strength, high velocity oxy fuel spraying, optimization, response surface methodology, WC-CrC-Ni coatings

## 1. Introduction

WC-based cermet coatings are widely used to protect materials from erosion and corrosion because of their ability to resist wear and corrosion (Ref 1). It is generally believed that high velocity of spray particles and improved melting benefits the adhesion of a coating on to a substrate. High Velocity Oxy-Fuel (HVOF) spray process is characterized by a high flame velocity up to 2000 m/s. Such high velocity flame consequently results in the formation of spray particle stream with high velocity compared to conventional flame spraying and plasma spraying. Accordingly, HVOF spray process is a promising thermal spray process to deposit coatings with low porosity, consequently high density and higher bond strength (Ref 2, 3).

Due to the high velocity associated with a relatively low flame temperature, HVOF process is suitable for producing cermet coatings of low porosity content (about 1%) with

denser and less oxidized cermet coatings than other thermal spray methods with no significant thermal and mechanical alterations of the substrate (Ref 4). Wang et al., investigated the factors influencing the bond strength of HVOF-sprayed coatings. The authors have mentioned that the conventional state parameters of spray particles including temperature, velocity, and momentum were not directly correlated with the bond strength of HVOF coatings. The physical properties of the non-melting phases in a two-phase particle significantly influence the bond strength of HVOF coatings (Ref 5).

Fang et al. (Ref 6), studied the effect of HVOF process parameters on the wear behavior of WC-CrC-Ni coatings using Taguchi technique. Maria et al. (Ref 7), discussed different techniques of optimization and characterization of HVOF coatings, and they opined that a deeper understanding of the spray process including starting materials, spray process, and particle-substrate interactions is required to produce good coating quality with suitable properties and required performance for specific applications.

Conversely, optimization of HVOF spray process involving multiple factors and multiple responses has not yet been reported in the literature. Hence, this investigation deals with the application of response surface methodology (RSM) in developing empirical relationships to estimate the adhesion bond strength and the lap shear bond strength of the WC-CrC-Ni coatings and optimizing HVOF spray process parameters, incorporating important HVOF spray parameters, namely, oxygen flow rate ( $O$ ), LPG flow rate ( $L$ ), standoff distance ( $S$ ), powder feed rate ( $F$ ), and carrier gas flow rate ( $C$ ).

## 2. Methodology of Investigation

In order to achieve the desired objectives, the present investigation was planned as depicted in the flow chart (Fig. 1).

C. Thiruvikraman, Department of Manufacturing Engineering, Annamalai University, Annamalainagar (P.O.), Chidambaram 608 002, India; V. Balasubramanian, Centre for Materials Joining and Research (CEMAJOR), Department of Manufacturing Engineering, Annamalai University, Annamalainagar (P.O.), Chidambaram 608 002, India; and K. Sridhar, Marine Materials Department, Naval Materials Research Laboratory (NMRL), Ambernath (P.O.), Thane 421 506, India. Contact e-mails: visvabalu@yahoo.com, ctvikraman@gmail.com and sridsudi@gmail.com.

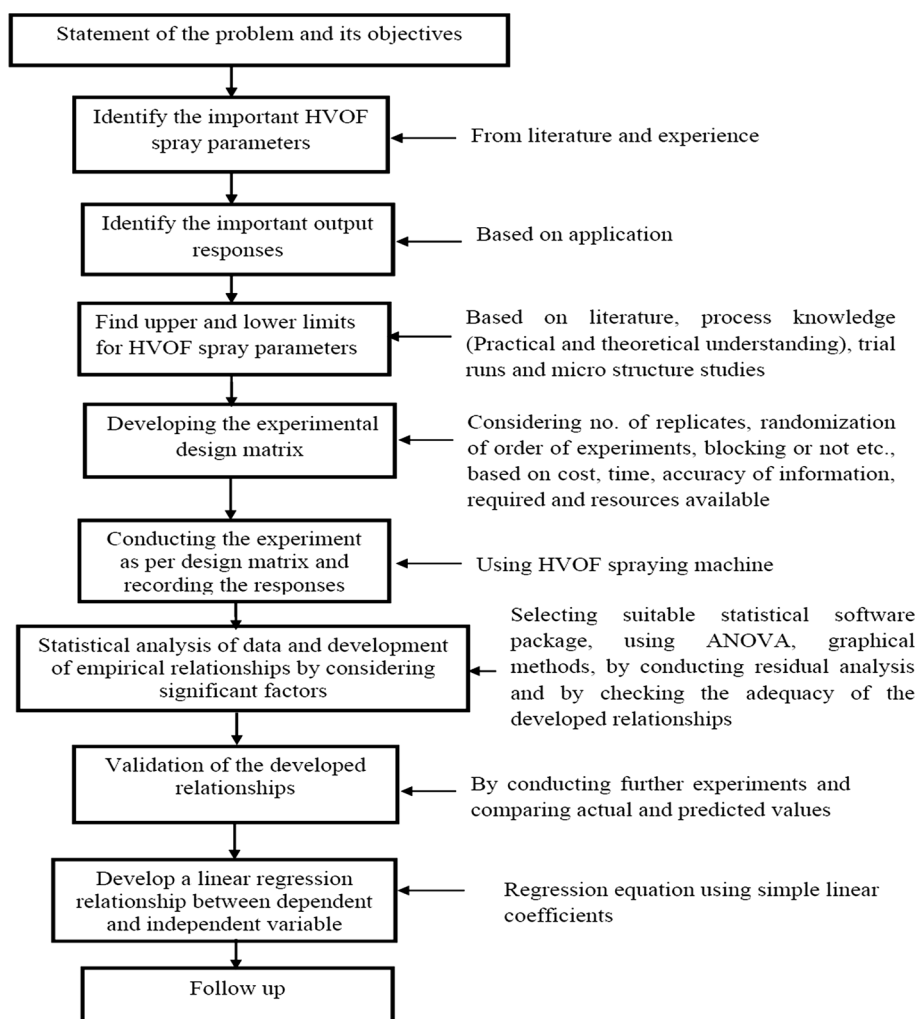


**Fig. 1** Flow chart depicting the methodology of investigation

## 2.1 Identifying the Important Spray Parameters

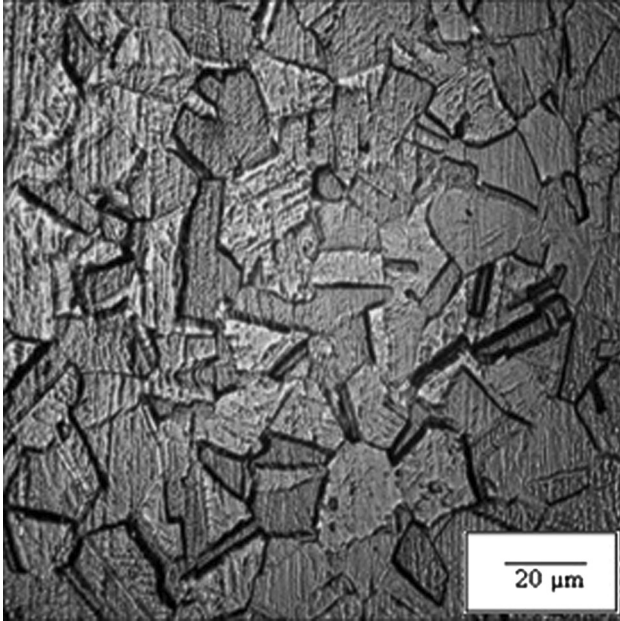
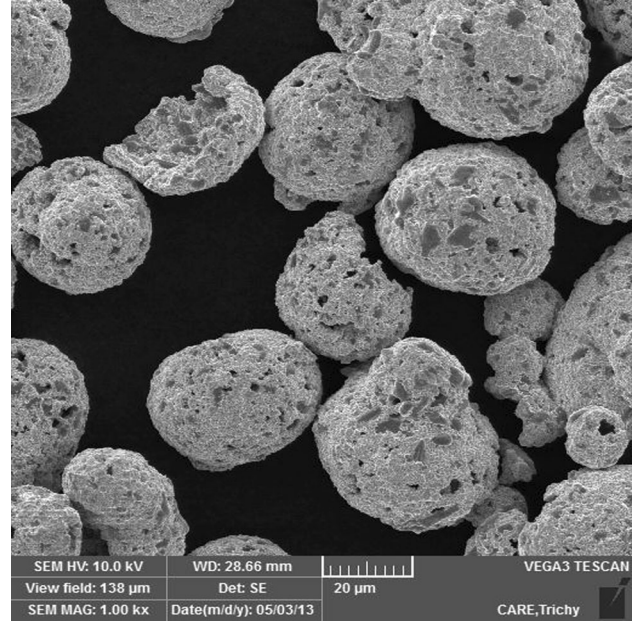
Preliminary step in the design of experiments is to select variables of the process under investigation. It has been widely recognized that in the thermal spray community, there are many hundreds of parameters, which can potentially influence the properties of the coatings. For economic (time requirements) and theoretical reasons (interdependence of parameters), it is not possible to control all possible parameter variations. From the literature (Ref 8-10) and the previous work done in our laboratory, the predominant HVOF spray parameters which are having a greater influence on coating characteristics were identified, and they are oxygen flow rate, fuel flow rate, powder feed rate, carrier gas flow rate, and spray distance. These are the primary operational parameters contributing to the melting and flattening of the powder particles, subsequently, influencing the coating characteristics of HVOF-sprayed WC-Cr<sub>3</sub>C<sub>2</sub>-Ni coatings.

## 2.2 Finding the Working Limits of the Parameters

A large number of spraying trials were conducted on grit-blasted 5-mm-thick AISI 304L stainless steel substrate coupons to determine the feasible working range of the above factors by varying one of the HVOF spray parameters and keeping the rest of them at a constant value. The chemical composition of the substrate material was found by optical emission spectroscopy method and is presented in Table 1. The microstructure of the base metal is displayed in Fig. 2. The feedstock was agglomerated and sintered WC-20% Cr<sub>3</sub>C<sub>2</sub>-7% Ni powder (H.C. Starck, Germany, Amperit 551.074) with an average particle size of  $45 \pm 15 \mu\text{m}$  as shown in Fig. 3. As a result of its spherical particle shape, it also showed a very good flowability during spraying. The WC-Cr<sub>3</sub>C<sub>2</sub>-Ni powder was directly sprayed on to the grit-blasted substrate without any bond coat. HVOF spraying was carried out using HIPOJET 2700 gun (Make: MECPL, Jodhpur, India). Different combinations of HVOF process parameters were used to carry out the

**Table 1** Chemical compositions (wt.%) of substrate material and coating material

Material	C	Mn	P	S	Si	Cr	Ni	O	Fe	W
SS 304L	0.017	1.81	0.025	0.04	0.22	18.59	8.66	...	Bal	...
WC-Cr <sub>3</sub> C <sub>2</sub> -Ni	7.0	...	...	...	...	20	7.0	0.2	0.3	Bal

**Fig. 2** Optical micrograph of substrate material (AISI 304L SS)**Fig. 3** Scanning electron micrograph of WC-Cr<sub>3</sub>C<sub>2</sub>-Ni powder

trial runs. Coating thickness of all the deposits was maintained at  $300 \pm 25 \mu\text{m}$ . To fix the limits of the considered factors, a couple of criteria were adopted. The criteria were that the coatings must have minimum tensile bond strength of 4 MPa, and they must be deposited with a minimum deposition efficiency of 35%. During the trials, the following observations were made.

- (i) If the spray was carried out below 242 lpm oxygen flow rate, then poor adhesion and subsequent delamination of the coating were observed (Fig. 4a). If the oxygen flow rate was increased beyond 258 lpm, then horizontal and vertical cracking occurred due to escaping of vapor entrapped in the deposit (Fig. 4b).
- (ii) If the fuel flow rate was below 52 lpm, then larger pore defects were observed (Fig. 4c), and if it was above 68 lpm, then bouncing up of unmelted particles was observed (Fig. 4d).
- (iii) If the standoff distance was less than 204 mm, then the distortion of the substrate and lamellae of the coating solidified with columnar shape were observed (Fig. 4e), and if it was increased beyond 252 mm, then re-solidification of the molten particles resulting in poor coating adhesion and poor deposition efficiency was observed (Fig. 4f).
- (iv) If the powder feed rate was less than 28 gpm, then lower deposition of the coating was observed

(Fig. 4g). If the powder feed rate was increased beyond 48 gpm, then a large fraction of the powder particles remains in the no molten condition, consequently, resulting in low spray deposition efficiency and coating delamination (Fig. 4h).

- (v) If the carrier gas flow rate was below 11 lpm, then the powder could not flow through the combustion gases, and if it was increased beyond 15 lpm, then the powder passed quickly through the combustion gases resulting in lower dwell time of powder in the combustion chamber, consequently poor melting of the powder.
- (vi) In our investigation during spray trials, we varied the substrate surface roughness ( $R_a$ ) from 3, 4, 5, 6, and  $7 \mu\text{m}$ , evaluated the bonding strength of the coating and we found that at  $R_a \approx 5 \mu\text{m}$  yielded better results. Thus, we have fixed the  $R_a \approx 5 \mu\text{m}$  as a constant for all our experiments in order to reduce the number of runs.
- (vii) Here, we are optimizing the spray parameters to coat naval components, where preheating of substrate will result in adverse effects, and hence, we have not considered preheating as a variable.

It is difficult to set up the process control due to the involvement of many parameters in the HVOF spray process. There is an associated cost to optimize the HVOF spray parameters for new coating materials. Therefore,



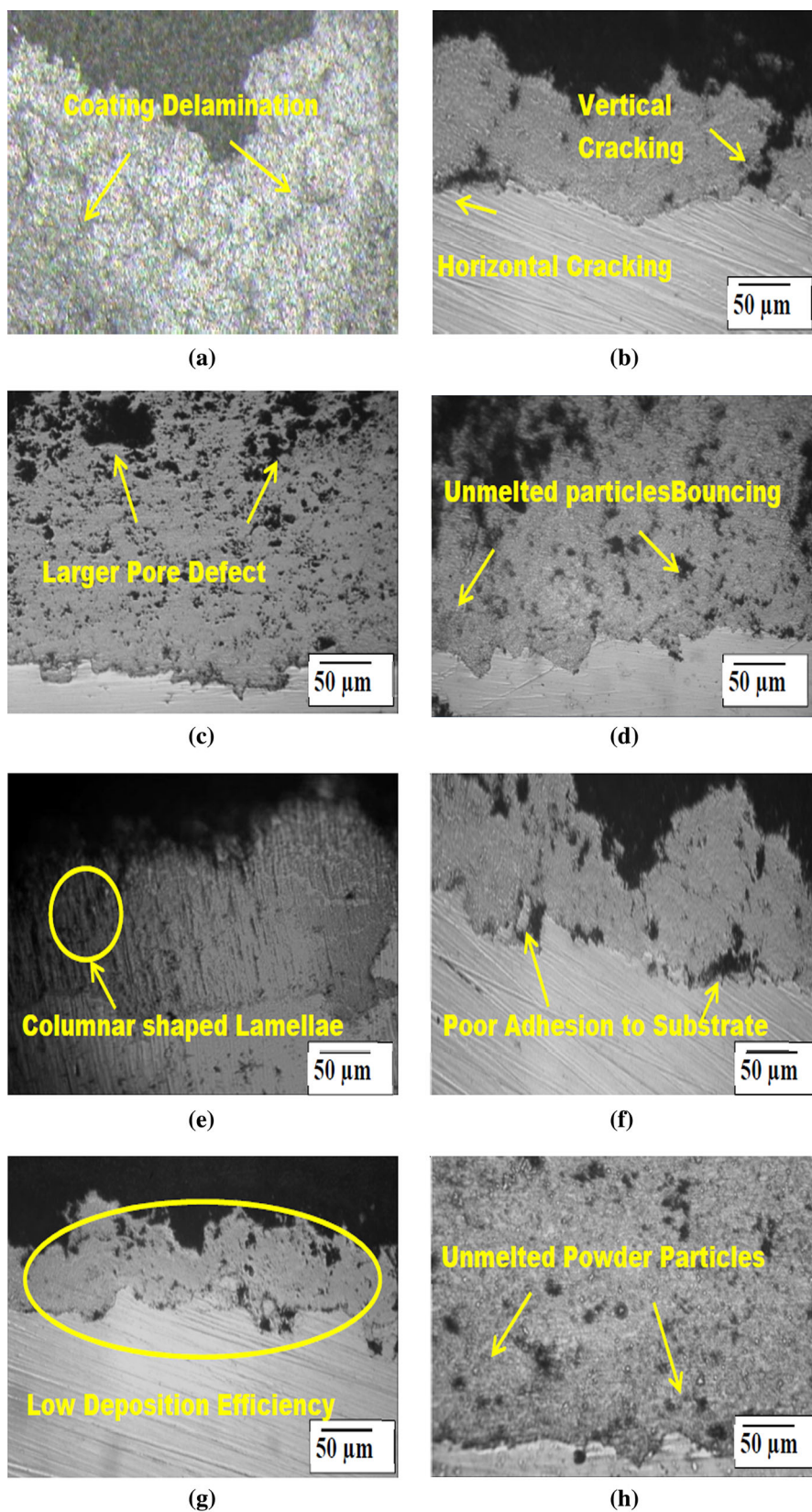


**Fig. 4** Optical micrographs of HVOF-sprayed WC-CrC-Ni coating. (a) Oxygen flow rate >242 lpm, (b) Oxygen flow rate <258 lpm, (c) Fuel flow rate >52 lpm, (d) Fuel flow rate <68 lpm, (e) Standoff distance >204 mm, (f) Standoff distance <252 mm, (g) Powder feed rate >28 gpm, (h) Powder feed rate <48 gpm



there is a need to reduce the variables in manageable numbers. The molten powder particles flattening and splat formation are sensitive to the processing parameters (Ref 11), especially for the oxygen flow rate, fuel flow rate, standoff distance, carrier gas flow rate, and the powder feed rate. In this work, the above spray parameters were chosen for investigation, mainly because these parameters can be directly measured and easier to control in real-time.

### 2.3 Developing the Experimental Design Matrix

By considering all the above conditions, the feasible working limits of the parameters were chosen in such a

way that HVOF spray deposition was carried out to deposit coatings without defects on the substrate. The range of individual factors was wide, hence a central composite rotatable five factor, five level design matrix was selected. The chosen spray parameters and their levels are presented in Table 2. The experimental design matrix consists of 32 sets of coded condition. The first 16 experimental conditions are derived from a half factorial experimental design; eight center points and eight star points were used Table 3. The method of designing such a matrix is dealt with elsewhere (Ref 12, 13). Linear, quadratic, and two-way interactive effects of the variables on the HVOF-sprayed WC-CrC-Ni coatings can be estimated from the

**Table 2 Important HVOF spray parameters and their levels**

No.	Parameters	Notations	Units	Levels				
				-2 Lowest	-1 Lower	0 Center	1 Higher	2 Highest
1	Oxygen flow rate	<i>O</i>	lpm	242	246	250	254	258
2	LPG flow rate	<i>L</i>	lpm	52	56	60	64	68
3	Powder feed rate	<i>F</i>	gpm	28	33	38	43	48
4	Spray distance	<i>S</i>	mm	204	216	228	240	252
5	Carrier gas flow rate	<i>C</i>	lpm	11	12	13	14	15

**Table 3 Design matrix and experimental results**

S.No	Coded value					Original value					Responses	
	<i>O</i>	<i>L</i>	<i>S</i>	<i>F</i>	<i>C</i>	<i>O</i> , lpm	<i>L</i> , lpm	<i>S</i> , mm	<i>F</i> , gpm	<i>C</i> , lpm	Adhesion bond strength, MPa	Lap shear bond strength, MPa
1	-1	-1	-1	-1	1	242	52	216	28	14	24	4
2	1	-1	-1	-1	-1	258	52	216	28	12	46	7
3	-1	1	-1	-1	-1	242	68	216	28	12	35	4
4	1	1	-1	-1	1	258	68	216	28	14	57	9
5	-1	-1	1	-1	-1	242	52	240	28	12	27	2
6	1	-1	1	-1	1	258	52	240	28	14	25	2
7	-1	1	1	-1	1	242	68	240	28	14	34	4
8	1	1	1	-1	-1	258	68	240	28	12	48	5
9	-1	-1	-1	1	-1	242	52	216	48	12	27	2
10	1	-1	-1	1	1	258	52	216	48	14	35	4
11	-1	1	-1	1	1	242	68	216	48	14	24	4
12	1	1	-1	1	-1	258	68	216	48	12	43	6
13	-1	-1	1	1	1	242	52	240	48	14	21	2
14	1	-1	1	1	-1	258	52	240	48	12	27	2
15	-1	1	1	1	-1	242	68	240	48	12	29	2
16	1	1	1	1	1	258	68	240	48	14	32	6
17	-2	0	0	0	0	234	60	228	38	13	24	2
18	2	0	0	0	0	266	60	228	38	13	51	7
19	0	-2	0	0	0	250	44	228	38	13	22	2
20	0	2	0	0	0	250	76	228	38	13	48	7
21	0	0	-2	0	0	250	60	204	38	13	56	6
22	0	0	2	0	0	250	60	252	38	13	35	2
23	0	0	0	-2	0	250	60	228	18	13	49	7
24	0	0	0	2	0	250	60	228	58	13	35	4
25	0	0	0	0	-2	250	60	228	38	11	47	5
26	0	0	0	0	2	250	60	228	38	15	36	7
27	0	0	0	0	0	250	60	228	38	13	57	8
28	0	0	0	0	0	250	60	228	38	13	62	9
29	0	0	0	0	0	250	60	228	38	13	58	8
30	0	0	0	0	0	250	60	228	38	13	60	9
31	0	0	0	0	0	250	60	228	38	13	62	8
32	0	0	0	0	0	250	60	228	38	13	64	9

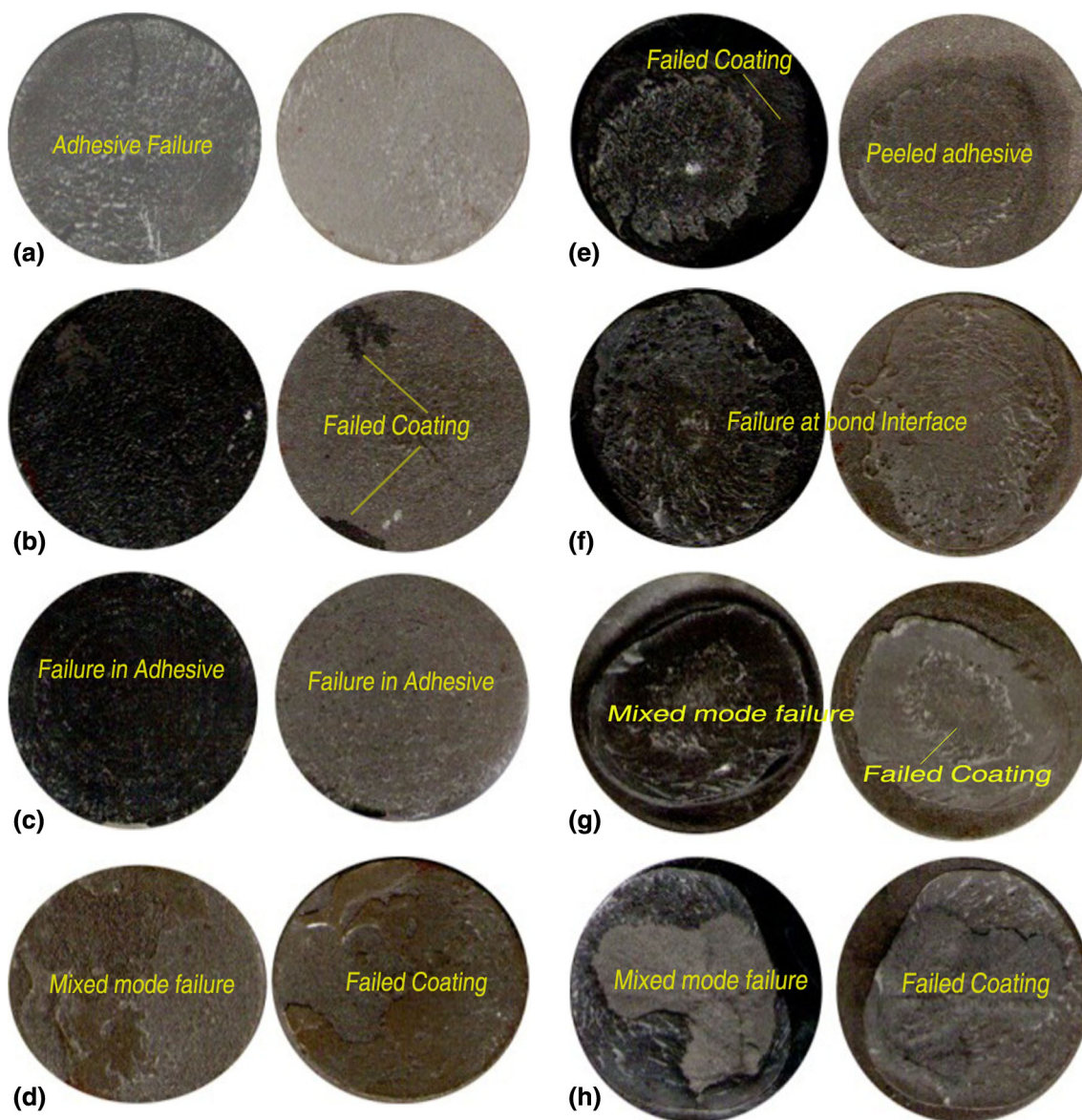


**Fig. 5** Scanned images of adhesion bond test failed specimens at various spray conditions. (a) Spray condition 4, (b) Spray condition 8, (c) Spray condition 12, (d) Spray condition 16, (e) Spray condition 20, (f) Spray condition 24, (g) Spray condition 28, (h) Spray condition 32

above 32 experiments. The upper and lower levels of the factors are coded as +2 and -2 respectively for the convenience of processing the experimental data. The coded values of any intermediate value can be calculated using the following relationship (Ref 13).

$$X_i = 2[2X - (X_{\max} + X_{\min})]/(X_{\max} - X_{\min}), \quad (\text{Eq 1})$$

where  $X_i$  is the required coded value of a variable  $X$ ,  $X$  is any value of the variable from  $X_{\min}$  to  $X_{\max}$ ,  $X_{\min}$  is the lower level of the variable, and  $X_{\max}$  is the highest level of the variable.

To evaluate the coating properties, two geometries of coated substrates were used:

- (i) 25.4 mm × 25.4 mm (diameter × height) cylindrical specimens for tensile bond strength test.
- (ii) 25.4 × 76.2 × 5 mm flats for lap shear bond strength test. Surface preparation was done with grit blasting before HVOF spraying. Grit blasting was carried out using corundum grits of size of  $500 \pm 320 \mu\text{m}$  and subsequently degreased using acetone in an ultrasonic bath and dried. After grit blasting, the average surface



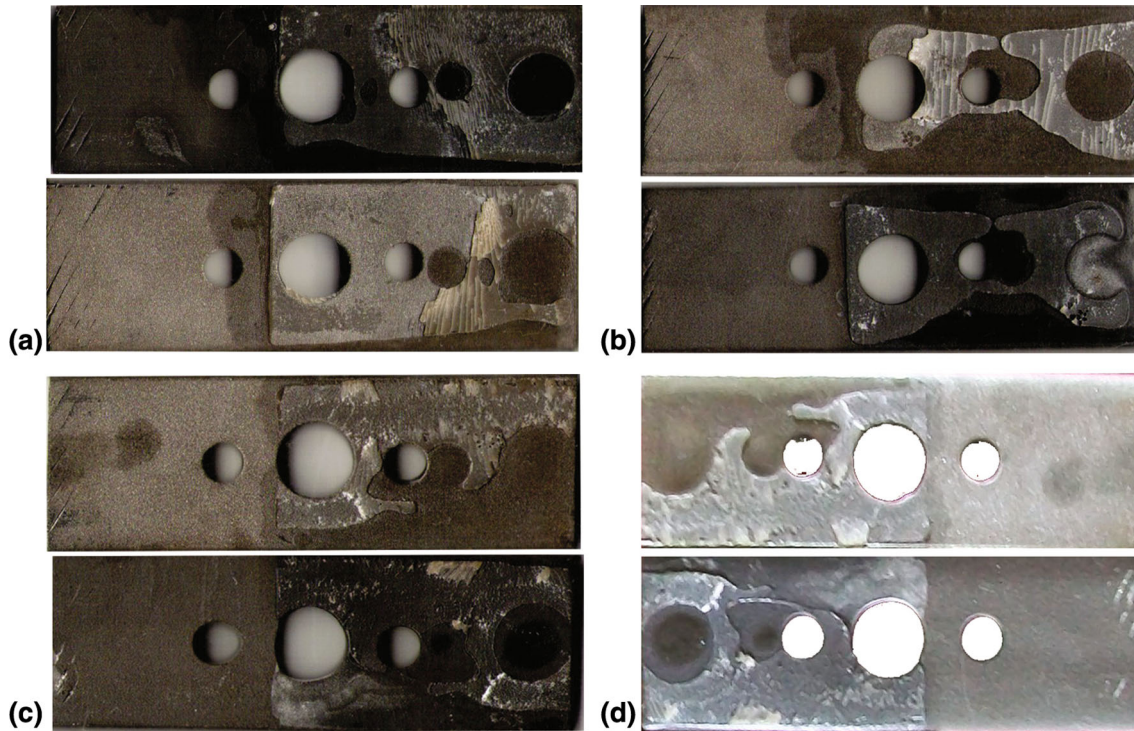


**Fig. 6** Scanned images of lap shear bond test failed specimens at various spray conditions. (a) Spray condition 8, (b) Spray condition 16, (c) Spray condition 24, (d) Spray condition 32

roughness was measured using the surface roughness tester (Make: Mitutoyo, Japan; Model: Surftest 301), and it was maintained at  $\approx 5 \mu\text{m}$  level.

## 2.4 Recording the Responses

The adhesion bond strength test was carried out as per ASTM C 633 standard, and the lap shear bond strength test was carried out as per EN 1465 standard using a universal testing machine (Make: FIE Blue Star, India; Model: UNITEK-94100). For each experimental condition, three coated specimens were prepared and tested to minimize experimental errors. A special purpose heat curable epoxy, HTK ULTRA BOND-100, Supplied by Metallizing Equipment Corporation (MEC-PL), Jodhpur, India and imported from HTK Hamburg GmbH, Germany. Glue is heat cured at  $190^\circ\text{C}$  for approx. 35 min with an applied load of  $70 \text{ N/cm}^2$ . The tensile bond strength and lap shear bond strength values of the epoxy were found to be 70 and 34 MPa, respectively. Scanned images of the failed specimens during the adhesion bond test and lap shear bond strength test were shown in (Fig. 5 and 6), respectively. From Fig. 5, it could be inferred that a few of the bond test specimens present partial (combined adhesive and cohesive) coating failures. The basic bond strength was evaluated by the degree of coverage of the remaining particles which remain bonded even after the testing of bonding strength. Hence, whenever a bond test presented a partial failure like those shown in Fig. 5(d) and (h), the true bond strength was evaluated from that coating area remaining

on the substrate after the test, which was intact and did not detach or fail (Ref 14).

## 2.5 Developing Empirical Relationships

In order to correlate the HVOF spray parameters and the coating characteristics, a second-order quadratic model was developed to predict the responses based on the experimentally measured values. The responses adhesion bonding strength and lap shear strength are functions of oxygen flow rate ( $O$ ), LPG flow rate ( $L$ ), powder feed rate ( $F$ ), spray distance ( $S$ ), and carrier gas flow rate ( $C$ ), and it can be expressed as

$$\text{Responses} = f(O, L, S, F, C) \quad (\text{Eq 2})$$

The second-order polynomial (regression) equation used to represent the response surface  $Y$  is given by

$$Y = b_0 + \sum b_i x_i + \sum b_{ii} x_i^2 + \sum b_{ij} x_i x_j \quad (\text{Eq 3})$$

For the five factors, the selected polynomial can be expressed as

$$Y = \{b_0 + b_1(O) + b_2(L) + b_3(S) + b_4(F) + b_5(C) + b_{12}(OL) + b_{13}(OS) + b_{14}(OF) + b_{15}(OC) + b_{23}(LS) + b_{24}(LF) + b_{25}(LC) + b_{11}(O^2) + b_{22}(L^2) + b_{33}(S^2) + b_{44}(F^2) + b_{55}(C^2)\}, \quad (\text{Eq 4})$$

where  $b_0$  is the average of the responses, and  $b_1, b_2, b_3, \dots, b_{33}$  are regression coefficients that depend on



respective linear, interaction, and squared terms of factors. In order to estimate the regression coefficients, a number of experimental design techniques are available. In this work, central composite rotatable design (Table 3) was used, which fits the second-order response. All the coefficients were obtained by applying central composite rotatable design using the Design-Expert statistical software package (version 8.07.1). The significance of each coefficient was determined by Student's  $t$  test and  $p$  values, which are listed in Tables 4 and 5. In this case  $O$ ,  $L$ ,  $S$ ,  $F$ ,  $C$ ,  $OL$ ,  $OS$ ,  $LF$ ,  $LC$ ,  $SF$ ,  $O^2$ ,  $L^2$ ,  $S^2$ ,  $F^2$ , and  $C^2$  are significant model terms. Values of "Prob > F" less than 0.0500 indicate that model terms are significant. Values greater than 0.10 indicate that model terms are not significant. After determining the significant coefficients (at 95% confidence level), the final empirical relationship was constructed using only these coefficients, and the final mathematical model to estimate adhesion bond strength (ABS) and lap shear bond strength (LSBS) are given below:

$$\begin{aligned} \text{ABS} = & [60.84 + 6.08O + 5.08L - 3.75S - 3.58F \\ & - 2.17C - 3.12OS - 2.12LF - 6.09O^2 \\ & - 6.72L^2 - 4.09S^2 - 4.97F^2 - 5.09C^2] \text{MPa} \end{aligned} \quad (\text{Eq 5})$$

$$\begin{aligned} \text{LSBS} = & [8.49 + 1.13O + 1.04L - 0.96S - 0.62F \\ & + 0.37C + 0.44OL - 0.44OS + 0.44LC \\ & + 0.44SF - 0.99O^2 - 0.99L^2 - 1.11S^2 \\ & - 0.74F^2 - 0.61C^2] \text{MPa}. \end{aligned} \quad (\text{Eq 6})$$

## 2.6 Checking Adequacy of the Developed Model

Analysis of variance (ANOVA) technique was used to check the adequacy of the developed empirical relationships. In this investigation, the desired level of confidence was considered to be 95%. The relationship may be considered to be adequate provided that

- the calculated value of the  $F$  ratio of the model developed should not exceed the standard tabulated value of  $F$  ratio, and
- the calculated value of the  $R$  ratio of the developed relationship should exceed the standard tabulated value of  $R$  ratio for a desired level of confidence.

It is found that the model is adequate. The 'model'  $F$  value of adhesion strength implies that the model is

**Table 4 ANOVA test results for adhesion bonding strength**

Source	Sum of squares	Df	Mean square	F value	p value prob > F	
Model	5924.08	20	296.20	29.24	<0.0001	Significant
<i>O</i> -oxygen flow rate	888.17	1	888.17	87.68	<0.0001	
<i>L</i> -LPG flow rate	620.17	1	620.17	61.22	<0.0001	
<i>S</i> -standoff distance	337.50	1	337.50	33.32	0.0001	
<i>F</i> -powder feed rate	308.17	1	308.17	30.42	0.0002	
<i>C</i> -carrier gas flow rate	112.67	1	112.67	11.12	0.0067	
<i>OL</i>	36.00	1	36.00	3.55	0.0861	
<i>OS</i>	156.25	1	156.25	15.43	0.0024	
<i>OF</i>	25.00	1	25.00	2.47	0.1445	
<i>OC</i>	0.000	1	0.000	0.000	1.0000	
<i>LS</i>	16.00	1	16.00	1.58	0.2349	
<i>LF</i>	72.25	1	72.25	7.13	0.0218	
<i>LC</i>	12.25	1	12.25	1.21	0.2949	
<i>SF</i>	4.00	1	4.00	0.39	0.5426	
<i>SC</i>	4.00	1	4.00	0.39	0.5426	
<i>FC</i>	0.25	1	0.25	0.025	0.8780	
$O^2$	1088.24	1	1088.24	107.43	<0.0001	
$L^2$	1323.03	1	1323.03	130.61	<0.0001	
$S^2$	490.91	1	490.91	48.46	<0.0001	
$F^2$	723.37	1	723.37	71.41	<0.0001	
$C^2$	760.24	1	760.24	75.05	<0.0001	
Residual	111.42	11	10.13			
<i>Lack of fit</i>	75.92	6	12.65	1.78	0.2713	Not significant
<i>Pure Error</i>	35.50	5	7.10			
Cor total	6035.50	31				
Std. dev.	3.18					
Mean	40.63					
C.V. %	7.83					
PRESS	2025.85					
$R^2$	0.9815					
Adj $R^2$	0.9480					
Pred $R^2$	0.6643					
Adeq precision	16.046					

Terms in Italicized are coded spray parameters and important response terms  
df, degrees of freedom; CV, coefficient of variation;  $F$ , Fisher ratio;  $p$ , probability

**Table 5 ANOVA test results for lap shear strength**

Source	Sum of squares	Df	Mean square	F value	p value prob > F	
Model	197.6	20	9.88	41.46	<0.0001	Significant
<i>O</i> -oxygen flow rate	30.38	1	30.38	127.47	<0.0001	
<i>L</i> -LPG flow rate	26.04	1	26.04	109.28	<0.0001	
<i>S</i> -standoff distance	22.04	1	22.04	92.5	<0.0001	
<i>F</i> -powder feed rate	9.38	1	9.38	39.34	<0.0001	
<i>C</i> -carrier gas flow rate	3.38	1	3.38	14.16	0.0031	
<i>OL</i>	3.06	1	3.06	12.85	0.0043	
<i>OS</i>	3.06	1	3.06	12.85	0.0043	
<i>OF</i>	0.063	1	0.063	0.26	0.6187	
<i>OC</i>	0.56	1	0.56	2.36	0.1527	
<i>LS</i>	0.56	1	0.56	2.36	0.1527	
<i>LF</i>	0.063	1	0.063	0.26	0.6187	
<i>LC</i>	3.06	1	3.06	12.85	0.0043	
<i>SF</i>	3.06	1	3.06	12.85	0.0043	
<i>SC</i>	0.063	1	0.063	0.26	0.6187	
<i>FC</i>	0.56	1	0.56	2.36	0.1527	
<i>O</i> <sup>2</sup>	28.67	1	28.67	120.32	<0.0001	
<i>L</i> <sup>2</sup>	28.67	1	28.67	120.32	<0.0001	
<i>S</i> <sup>2</sup>	36.38	1	36.38	152.66	<0.0001	
<i>F</i> <sup>2</sup>	16	1	16	67.16	<0.0001	
<i>C</i> <sup>2</sup>	11.05	1	11.05	46.35	<0.0001	
Residual	2.62	11	0.24			
<i>Lack of Fit</i>	1.12	6	0.19	0.62	0.7109	Not significant
<i>Pure error</i>	1.5	5	0.3			
Cor total	200.22	31				
Std. dev.	0.49					
Mean	5.16					
C.V. %	9.47					
PRESS	32.13					
<i>R</i> <sup>2</sup>	0.9869					
Adj <i>R</i> <sup>2</sup>	0.9631					
Pred <i>R</i> <sup>2</sup>	0.8395					
Adeq precision	19.177					

Terms in Italicized are coded spray parameters and important response terms  
df, degrees of freedom; CV, coefficient of variation; *F*, Fisher ratio; *p*, probability

significant. The lack of fit *F* values implies that the lack of fit is insignificant. The Fisher's *F* test with a very low probability value ( $P_{\text{model}} > F = 0.0001$ ) demonstrates a very high significance. The goodness of fit of the model was checked by the determination coefficient (*R*<sup>2</sup>). The coefficient of determination (*R*<sup>2</sup>) was calculated to be 0.9915 for response adhesion strength. This implies that 99.15% of experimental data confirms the compatibility with the data predicted by the model, and the model does not only explain about 0.85% of the total variations (Ref 15). The *R*<sup>2</sup> value is always between 0 and 1, and its value indicates aptness of the model. For a good statistical model, *R*<sup>2</sup> value should be close to 1.0. The adjusted *R*<sup>2</sup> value reconstructs the expression with the significant terms. The value of the adjusted determination coefficient (Adj *R*<sup>2</sup>=0.9480) is also high to advocate for a high significance of the model. The Pred *R*<sup>2</sup> implies that the model could explain 95% of the variability in predicting new observations. This is in reasonable agreement with the Adj *R*<sup>2</sup> of shear strength analysis. The value of the coefficient of variation is also around 7.83 indicates that the deviations between experimental and predicted values are low. Adeq. precision measures the signal to noise ratio. A ratio greater than 4 is desirable. During this investigation, the ratio (16.046) indicates an adequate signal. This model can be used to navigate the design space and able to predict the

responses for a given input in coded form. Similarly, the ANOVA analysis of shear strength is presented in Table 5. From the table, it is understood that the developed statistical model was found to be adequate at 95% confidence level. Coefficient of determination "*R*<sup>2</sup>" was used to find how close the predicted and experimental values lie. The value of "*R*<sup>2</sup>" for the above-developed model was calculated and is presented in Tables 4 and 5, which indicates that a high correlation exists between estimated values and experimental values. Collectively, these results indicate the excellent capability of the regression model. Further, each observed value matches its experimental value well with minor variations, as shown in Fig. 7.

## 2.7 Verification of Developed Empirical Relationships

In the process of developing of empirical relationships, it is important to determine whether the developed model meets the specifications, and its outputs are correct. This is the process of verification and validation. Further, this model was validated by predicting and conducting experiments on three more spray parameter combinations that are not prescribed by in the design matrix (Table 3). The experimental and model response results are presented in

Table 6. The predicted values of adhesion bond strength and lap shear bond strength obtained using model equations are in good agreement with the experimental values, and only minor variations are observed. From the above results, it is concluded that the developed models were more capable to predict the required responses, when one wants to know the response based upon the spray parameters in the prevailing conditions.

### 3. Results and Discussion

#### 3.1 Perturbation Plots

The developed empirical relationships can be used effectively to predict the responses by substituting process

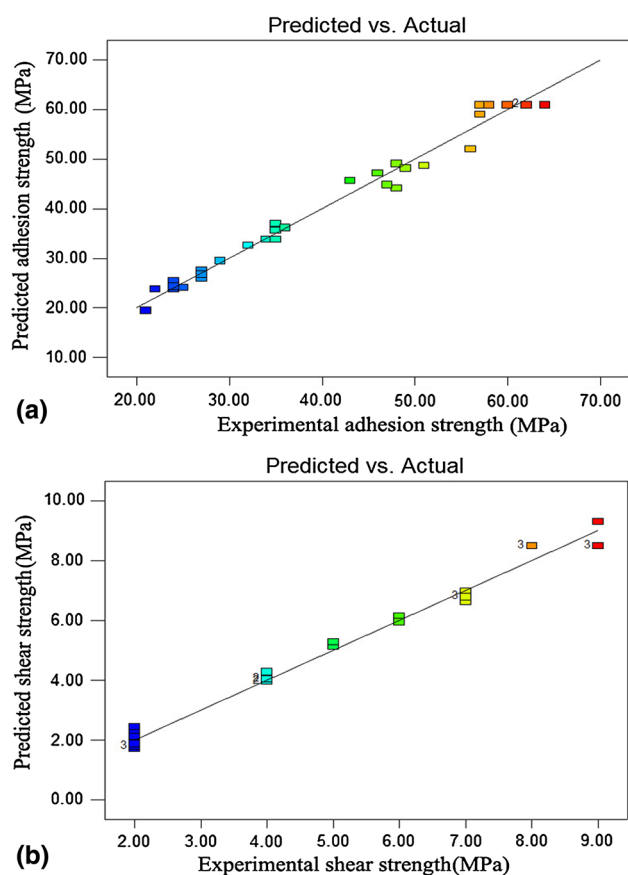


Fig. 7 Correlation graphs. (a) Adhesion bonding strength, (b) Lap shear bonding strength

Table 6 Verification results for the developed empirical relationships

Expt. No	O, lpm	L, lpm	S, mm	F, gpm	C, lpm	Adhesion bonding strength, MPa			Lap shear bonding strength, MPa		
						By expt	By model	Variation, %	By expt.	By model	Variation, %
1	244	54	208	30	11.5	25.2	24.2	-3.85	3.2	3.16	-1.25
2	248	58	212	33	12.5	28.3	27.6	-2.47	4.9	4.82	-3.21
3	251	62	225	35	13.2	31.8	33.2	4.40	6.1	6.4	4.92
4	256	65	232	40	13.5	33.2	32.3	-2.71	6.8	6.64	-2.35
5	257	67	245	45	14.5	23.4	24.1	2.99	2.7	2.8	3.70

parameter values in coded form. Based on these empirical relationships, the main and interaction effects of the process parameters on the coating properties were computed and plotted in the form of perturbation plots, as shown in Fig. 8. The perturbation plot is an important diagrammatic representation, which provides outline views of the response surface (Ref 16). The perturbation plot can be used to compare the effects of all factors at a specific point in the RSM design space. For response surface designs, the perturbation plot shows how the response changes as each factor moves from the selected reference point, while all other factors remain constant at the reference value. Normally, Design-Expert software sets the reference point

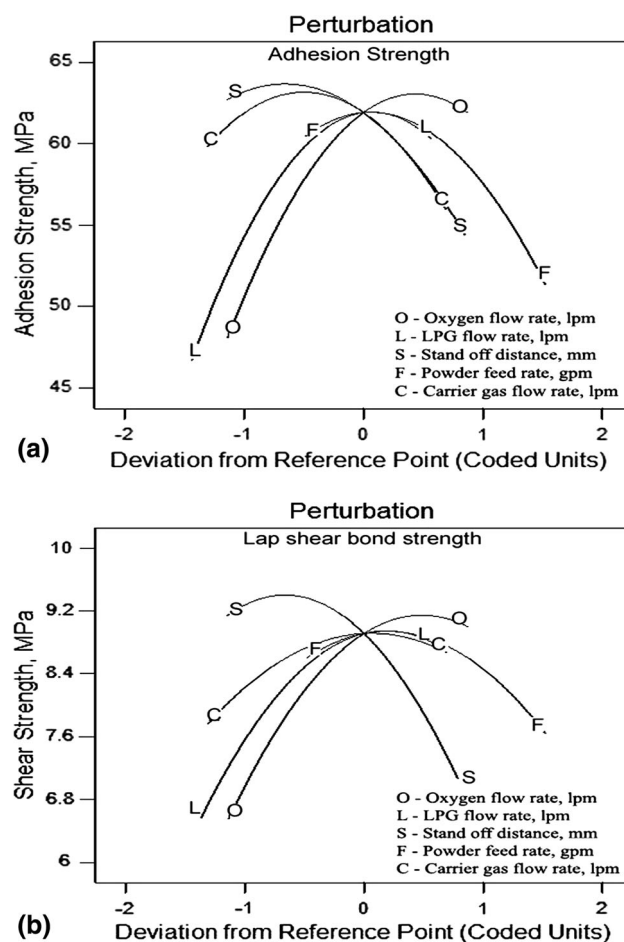


Fig. 8 Perturbation plots. (a) Adhesion bonding strength, (b) Lap shear bonding strength



default in the middle of the design space (the coded zero level of each factor) (Ref 17). A steep slope or curve in a factor shows that the response is sensitive in that factor. A relatively flat line shows insensitivity to change in that particular factor (Ref 18).

Further, using the  $F$  values, the predominant factors, which have the major and minor effects on the responses, could be assessed. From the  $F$  value assessment, it was found that the predominant factors which have direct influence on the responses as per hierarchy are oxygen flow rate, LPG flow rate, standoff distance, powder feed rate, and carrier gas flow rate. This pronounced effect also has been observed from Fig. 8(a) and (b) and shows good agreement with the predicted model  $F$  values.

### 3.2 Process Optimization

To investigate the influencing tendency of the HVOF spray process parameters on the responses, 3D graphs were plotted under certain processing conditions. The 3D response surface and 2D contour plots are the graphical representations of the regression equations used to determine the optimum values of the variables within the

ranges considered (Ref 19). Equation 5 (adhesion bond strength) is used to plot Fig. 9 (a)-(d) (surface plots) and 10(a)-(d) (contour plots). Equation 6 (shear strength) is used to plot Fig. 11(a)-(d) (surface plots) and 12(a)-(d) (contour plots). It is clear from Fig. 9(a)-(d) that the tensile bond strength increases, reaches an apex, and then decreases with the increase in the levels of the factors under consideration.

The apex of the response plot shows the maximum adhesion bond strength (the same trend was observed in the case of lap shear bond strength Fig. 11(a)-(d)). These response contours can help in the prediction of the responses for any zone of the experimental domain. The optimization module in design-expert searches for a combination of factor levels, which simultaneously satisfies the requirements placed (i.e., optimization criteria) on each of the responses and process factors (i.e., multiple response optimization) (Ref 20). Numerical and graphical optimization methods were used in this study by choosing the desired goals for each factor and response. The optimization process aims to combine the goals into an overall desirability function. The numerical optimization finds a point or more that maximize this function. However, in

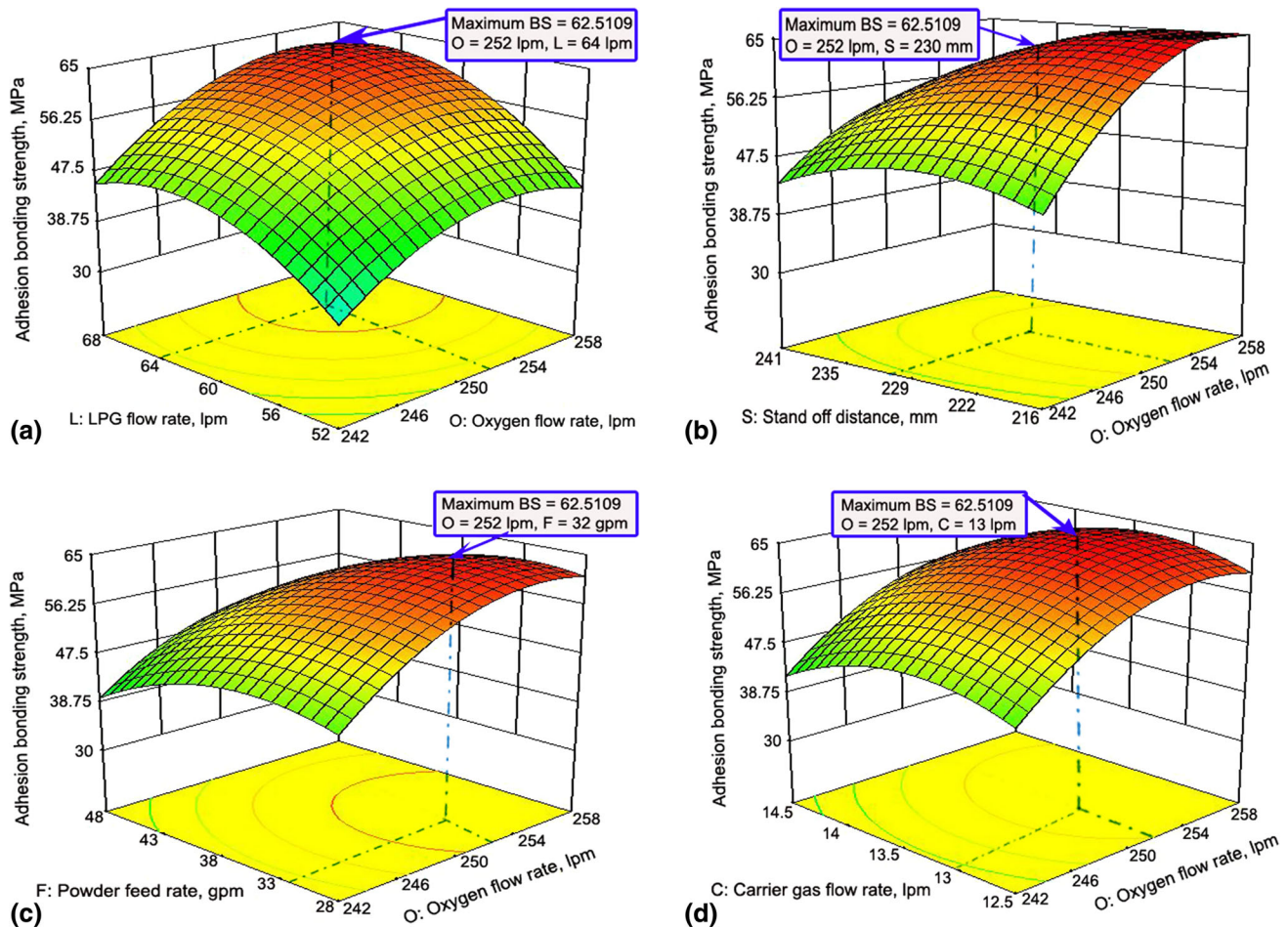


**Fig. 9** Surface plots for adhesion bonding strength. (a) Effect of  $O$  and  $L$ , (b) Effect of  $O$  and  $S$ , (c) Effect of  $O$  and  $F$ , (d) Effect of  $O$  and  $C$

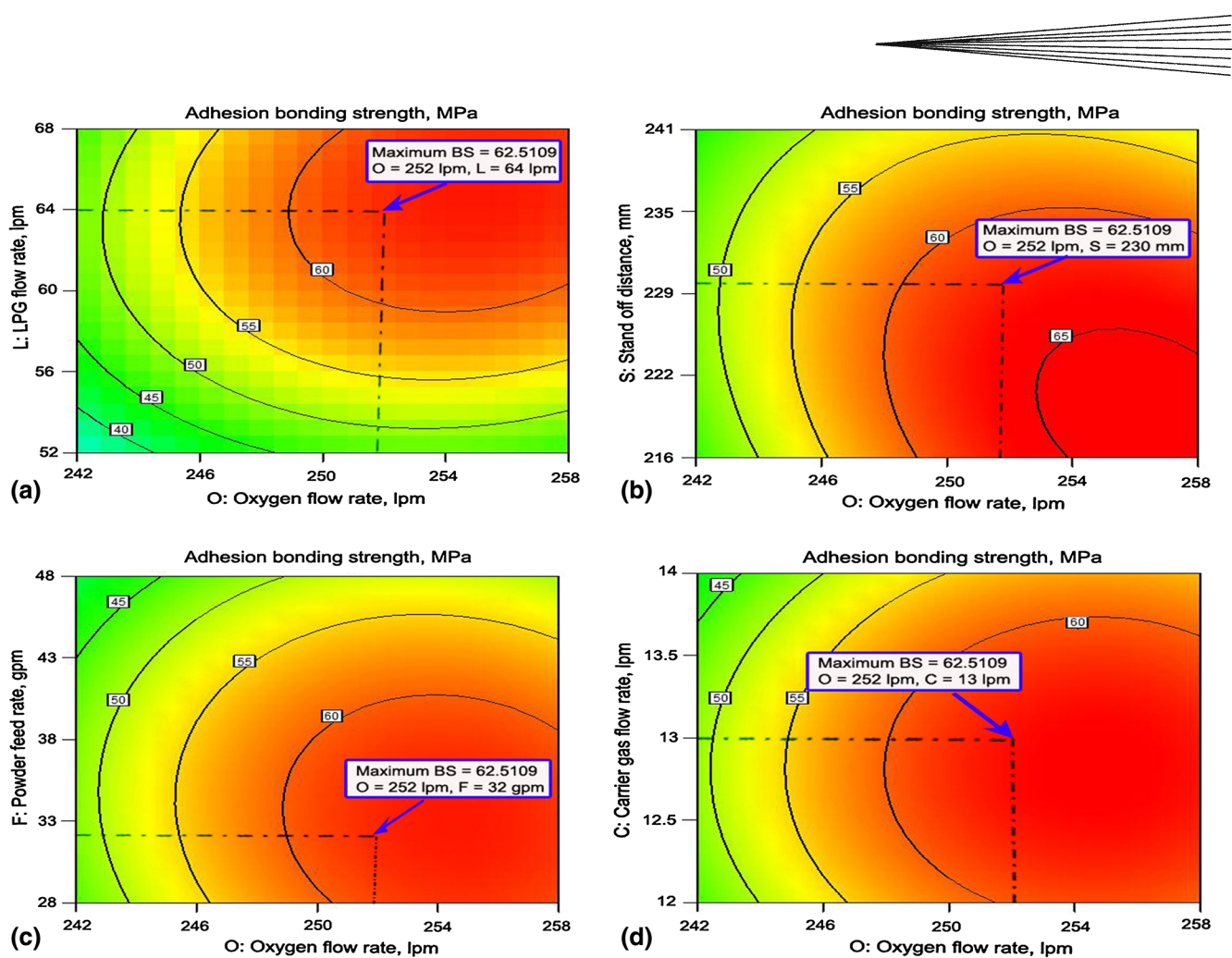


**Fig. 10** Contour plots for adhesion bonding strength. (a) Effect of *O* and *L*, (b) Effect of *O* and *S*, (c) Effect of *O* and *F*, (d) Effect of *O* and *C*

the graphical optimization with multiple responses, one has to define regions where requirements simultaneously meet the proposed criteria by superimposing or overlaying critical response contours on a contour plot. Then, visual search for the best compromise becomes possible.

In the case of dealing with many responses, it is recommended to perform numerical optimization first; otherwise, one may find it impossible to uncover a feasible region. The graphical optimization displays the area of feasible response values in the factor space. Regions that do not fit the optimization criteria are shaded (Ref 21). In the numerical optimization part, a criterion was adopted. The criterion is to maximize tensile bond strength and lap shear bond strength. In the case of graphical optimization for each response, the lower and/or upper limits have been chosen according to the numerical optimization results. The same criterion, which is proposed in the numerical optimization, was introduced in the graphical optimization.

Contour plots play a very important role in the study of a response surface. The contour plots are illustrated in Fig. 10(a)-(d) (adhesion bond strength) and 12(a)-(d) (Shear bond strength). Each contour curve represents an infinite number of combinations of values of two test

factors derived from the second-order quadratic equation within the considered range. The maximum predicted value is identified by the surface confined in the smallest ellipse or circle of the contour diagram. The circular contour plot indicates that the interactions between the corresponding factors are negligible, while the elliptical contour plot indicates that the interactions between the corresponding factors are significant (Ref 22). Furthermore, a contour plot is produced to display the region of the optimal factor settings visually. For second-order response surfaces, such a plot can be more complex compared to the simple series of parallel lines that can occur with first-order empirical relationships. Once the stationary point is found, it is usually necessary to characterize the response surface in the immediate vicinity of the point. Characterization involves identifying whether the stationary point found is a minimum response or maximum response or a saddle point. To classify this, it is more straightforward to examine it through a contour plot (Ref 23). By performing the numerical optimization, i.e., by solving Eq 4 and 5, analyzing the profile of the response surfaces and their corresponding contour plots (Fig. 10a-d and 12a-d), the response values are obtained.



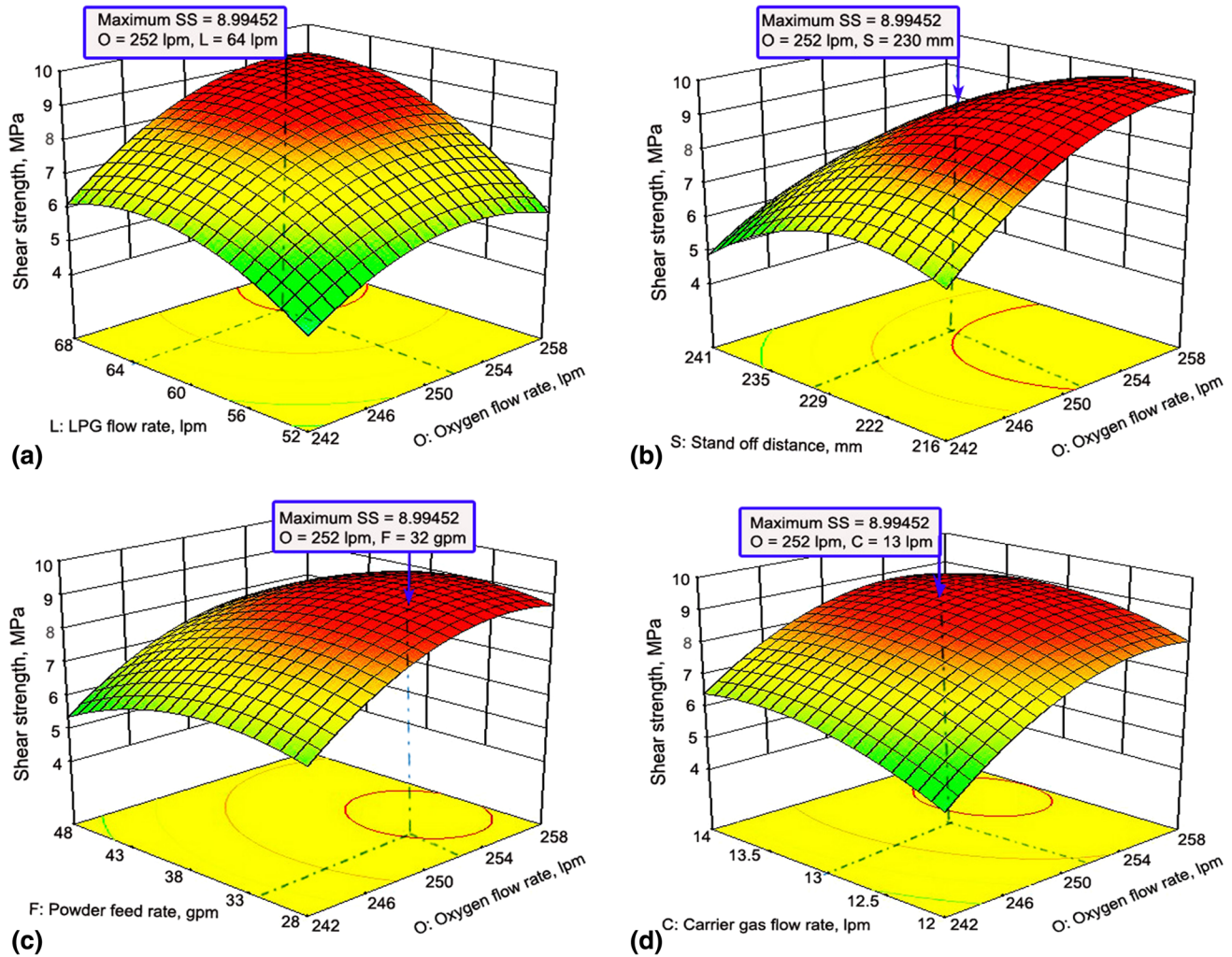


**Fig. 11** Surface plots for lap shear bonding strength. (a) Effect of  $O$  and  $L$ , (b) Effect of  $O$  and  $S$ , (c) Effect of  $O$  and  $F$ , (d) Effect of  $O$  and  $C$

The above mentioned response values could be achieved using the following optimized parameter settings: oxygen flow rate: 252 lpm, LPG flow rate: 64 lpm, standoff distance: 230 mm, powder feed rate: 32 gpm, and carrier gas flow rate: 13 lpm. The above values (factor values and response values) were also verified using the graphical optimization. The graphical optimization result allows visual inspection to choose the optimum coating condition. The shaded areas of the overlay plot are the regions that do not meet the proposed criteria (Ref 24). The graphical optimization plot is displayed in Fig. 13. To validate the model, three additional confirmation experiments were conducted to compare the experimental results with the prediction under the optimal conditions. The mean experimental response results are tabulated in Table 6. The validated response values show good agreement with the predicted values.

The optical micrograph of the cross section of the coating produced under optimized processing condition is shown in Fig. 14. From Fig. 14, it could be inferred that the microstructure of the coatings is strongly dependent

on processing conditions. When an adequately molten particle hits the substrate, the sudden deceleration causes a pressure build-up at the particle-substrate interface; the high pressure inside the particle forces the melted material to flow laterally or the ductile solid material to deform. The liquid spreads outward from the point of impact and forms a splat. The arresting of spreading results from the conversion of the particle kinetic energy into the work of viscous deformation and surface energy.

The process of splat formation depends on the velocity, size, molten state, chemistry, and angle of impact of the droplets on the surface. It is also subject to the surface topography of the substrate, its temperature, and reactivity (Ref 25). This process determines both microstructural and macroscopic characteristics of the coating. Optimum particle temperature corresponds to a decrease in the dynamic viscosity of the material, which together with optimum particle velocity, results in a higher degree of flattening. In addition, a higher degree of flattening corresponds to a decrease in splat thickness and a larger area of splat surface being in contact with the underlying



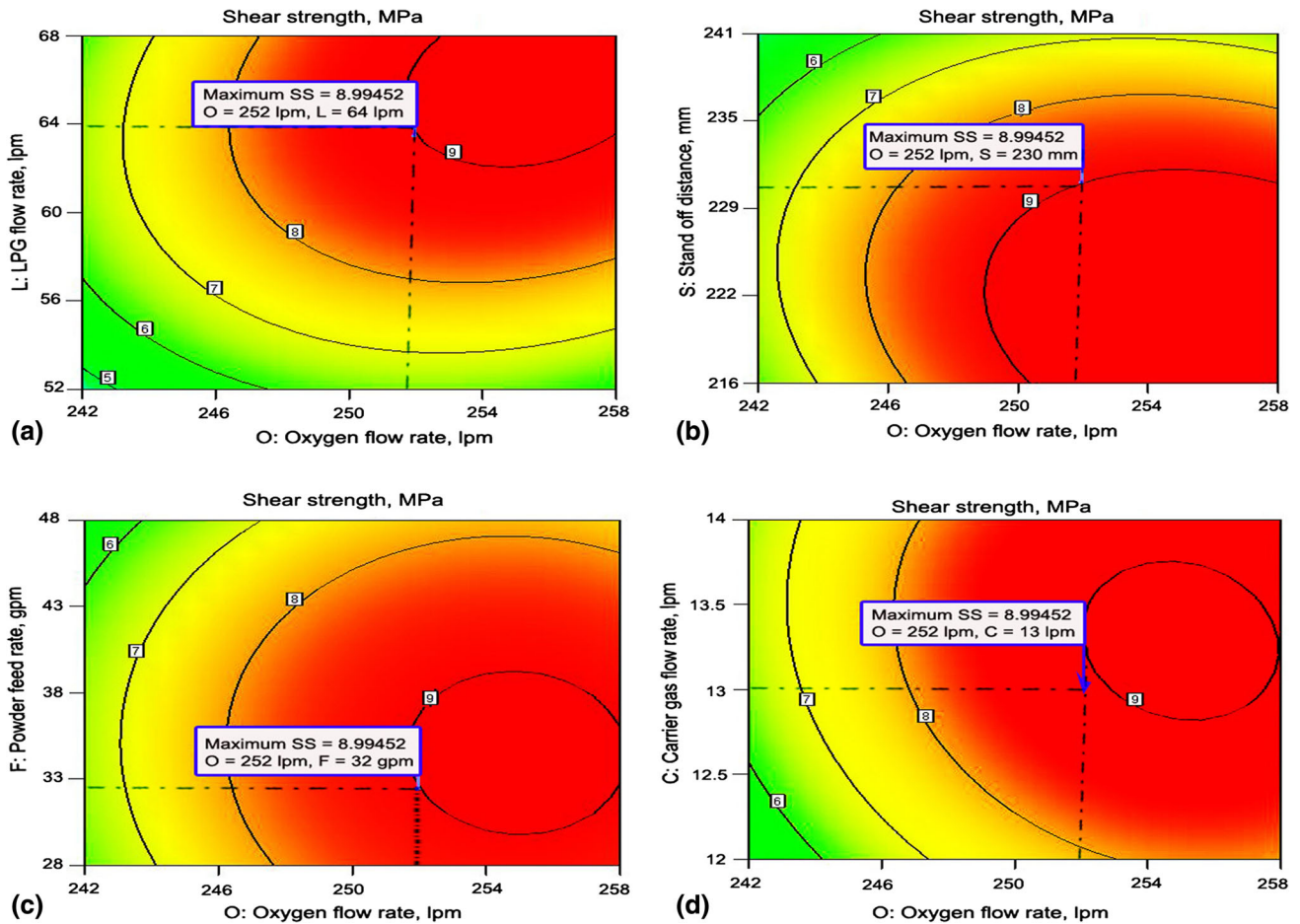


**Fig. 12** Contour plots for lap shear bonding strength. (a) Effect of  $O$  and  $L$ , (b) Effect of  $O$  and  $S$ , (c) Effect of  $O$  and  $F$ , (d) Effect of  $O$  and  $C$

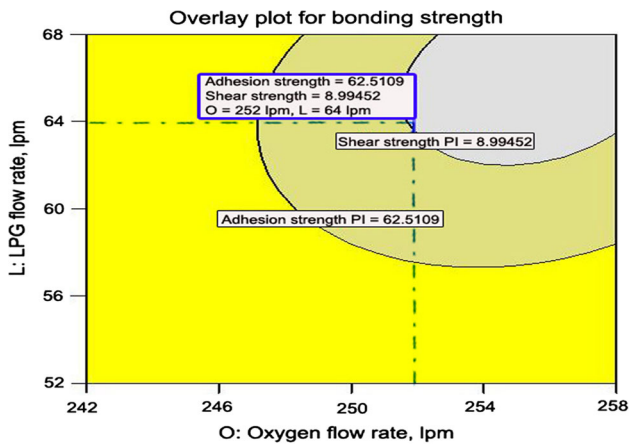


**Fig. 13** Overlay plot for bonding strength

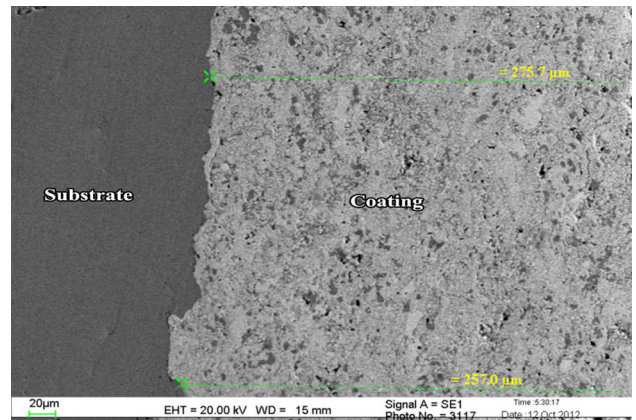


**Fig. 14** Scanning electron micrograph of HVOF-sprayed WC-CrC-Ni coating cross section at optimized spray condition

material (Ref 26), which leads to a higher deposition efficiency, bond strength, microhardness, and low porosity. In the case of the coating produced under optimum spray conditions, owing to adequate in-flight temperature, most particles undergo melting, so that each splat covers more

easily the surface topography onto which it flattens. The strength of WC-CrC-Ni cermet coatings sprayed under the optimum condition is the highest attainable bonding strength level. Under non-optimal conditions, attainable bonding strength was found to be low.

**Table 7 Validation results for optimization procedure**

HVOF spray parameters					Responses	
O, lpm	L, lpm	S, mm	F, gpm	C, lpm	Adhesion bonding strength, MPa	Lap shear bonding strength, MPa
248	60	220	30	11	54.71	6.34
<b>252</b>	<b>64</b>	<b>230</b>	<b>32</b>	<b>13</b>	<b>61.32</b>	<b>8.67</b>
256	66	240	34	15	56.54	5.98

Terms in bold are the optimized spray parameters

### 3.3 Validation of Optimization Procedures

The confirmation experiments were conducted with the HVOF spray process parameters as suggested by the numerical modeling (suggested solutions) and keeping the oxygen flow rate, LPG flow rate, powder feed rate spray distance, and carrier gas at 252 lpm, 64 lpm, 32 gpm, 230 mm, and 13 lpm, respectively. Minor difference was found between the predicted values and experimental values (Table 7). Further, two additional sets of experiments were conducted above and below the optimized HVOF spray process, parameters and observed results were presented in Table 7. From these results, it was inferred that deviating HVOF spray process parameters from the optimized conditions resulted in overmelting/poor melting of the powder particles due to the difference in air fuel ratio, variations in residence time of the powder particles in the flame, differences in spray distance and overdeposition/insufficient deposition of the powder particles on the substrate due to excess/deficient carrier gas flow, leading to the reduction in adhesion bonding strength and lap shear strength of the HVOF-sprayed WC-Cr<sub>3</sub>C<sub>2</sub>-Ni coatings.

## 4. Conclusions

1. Empirical relationships were developed to estimate the adhesion bond strength and lap shear bond strength of HVOF-sprayed WC-CrC-Ni coatings incorporating HVOF spray operational parameters.
2. From ANOVA test results (as per “F” value), it is found that the oxygen flow rate has greater influence on bonding strength and carrier gas flow rate has least influence on bonding strengths of the coatings.
3. The optimum deposition parameters yielded maximum adhesion bond strength and lap shear bond strength of HVOF-sprayed WC-CrC-Ni coatings are oxygen flow rate: 252 lpm, LPG flow rate: 64 lpm, standoff distance: 230 mm, powder feed rate: 32 gpm; and carrier gas flow rate: 13 lpm.

## Acknowledgments

The authors wish to express their sincere thanks to the Materials Panel, Naval Research Board (NRB), Ministry of Defense, Govt. of India, New Delhi for the financial

support extended to carry out this investigation through the sponsored Project No DNRD/05/4003/NRB/212. The authors wish to place their sincere thanks on record to The Director, Naval Materials Research Laboratory (NMRL), Ambarnath for extending facilities to characterize the coatings.

## References

1. I. Hussainova, Some Aspects of Solid Particle Erosion of Ceramics, *Tribol. Int.*, 2001, **34**, p 89-93
2. J. Mostaghimi, S. Chandra, R. Ghafouri-Azar, and A. Dolatabadi, Modelling Thermal Spray Coating Processes: A Powerful Tool in Design and Optimization, *Surf. Coat. Technol.*, 2003, **163-164**, p 1-11
3. J. Stokes and L. Looney, HVOF System Definition to Maximise the Thickness of Formed Components, *Surf. Coat. Technol.*, 2001, **148**, p 18-24
4. J.M. Perry, A. Neville, and T. Hodgkiess, A comparison of the Corrosion Behaviour of WC-CoCr and WC-Co HVOF Thermally Sprayed Coatings by In Situ Atomic Force Microscopy (AFM), *J. Therm. Spray Technol.*, 2002, **11**(4), p 536-541
5. Y.Y. Wang, C.J. Li, A. Ohmori, and Z. Frantisek, Examination of Factors Influencing the Bond Strength of High Velocity Oxy-Fuel Sprayed Coatings, *Surf. Coat. Technol.*, 2006, **200**, p 2923-2928
6. W. Fang, T.Y. Cho, J.H. Yoon, K.O. Song, S.K. Hur, S.J. Youn, and H.G. Chun, Processing Optimization, Surface Properties and Wear Behavior of HVOF Spraying WC-CrC-Ni Coating, *J. Mater. Process. Technol.*, 2009, **209**(7), p 3561-3567
7. M. Oksa, E. Turunen, Tomi. Suhonen, T. Varis, and S.-P. Hannula, Optimization and Characterization of High Velocity Oxy-Fuel Sprayed Coatings: Techniques, Materials, and Applications, *Coatings*, 2011, **1**, p 17-52
8. R.B. Hiemann, *Plasma-Spray Coating-Principles and Applications*, Wiley VCH Publishers Inc., New York, 1996
9. R. Suryanarayanan, *Plasma Spraying: Theory and Applications*, World Scientific Publishing, New York, 1993
10. L. Pawlowski, *The Science Engineering of Thermal Spray Coatings*, 2nd ed., John Wiley & Sons Ltd., London, 2008
11. E. Doring, R. Vaben, D. Stover, and D. Julich, The Influence of Spray Parameters on Particle Properties, *ITSC-International Thermal Spray Conf. (DVS-ASM)*, Paper 3, 2002, p. 440-448
12. R.G. Miller, J.E. Freund, and D.E. Johnson, *Probability and Statistics for Engineers*, Prentice of Hall of India Pvt. Ltd., New Delhi, 1999
13. D.C. Montgomery, *Design and Analysis of Experiments*, John Wiley & Sons Ltd., New Delhi, 2007
14. C.R.C. Lima and J.M. Guilemany, Adhesion Improvements of Thermal Barrier Coatings with HVOF Thermally Sprayed Bond Coats, *Surf. Coat. Technol.*, 2007, **201**, p 4694-4701
15. Standard Test Method for Adhesion or Cohesion Strength of Thermal Spray Coatings, C633, ASTM, Pennsylvania, 2010
16. Adhesives-Determination of Tensile Lap-Shear Strength of Rigid-to-Rigid Bonded Assemblies EN 1465, BS, 1995
17. Design-Expert Software, V8 User's Guide, *Technical Manual*, Stat Ease, Inc., Minneapolis, 2008



18. T. Troczynski and M. Plamondon, Response Surface Methodology for Optimization of Plasma Spraying, *J. Therm. Spray Technol.*, 1992, **1**, p 293-300
19. T. Valente, Statistical Evaluation of Vicker's Indentation Test Results for Thermally Sprayed Materials, *Surf. Coat. Technol.*, 1997, **90**, p 14-20
20. A.K. Lakshminarayanan, V. Balasubramanian, R. Varahamoorthy, and S. Babu, Predicting the Dilution of Plasma Transferred Arc Hardfacing of Stellite on Carbon Steel using Response Surface Methodology, *Met. Mater. Int.*, 2008, **14**, p 779-789
21. A.I. Khuri and J.A. Cornell, *Response Surfaces: Design and Analysis*, Marcel Dekker Ltd., New York, 1996
22. R.H. Myers and D.C. Montgomery, *Response Surface Methodology*, John Wiley & Sons Inc., New York, 2002
23. G.E.P. Box and N.R. Draper, *Empirical Model-Building and Response Surfaces*, John Wiley & Sons Inc, New York, 1986
24. R.A. Bailey, *Design of Comparative Experiments*, Cambridge University Press, New York, 2008
25. G. Bertrand, P. Bertrand, P. Roy, C. Rio, and R. Mevrel, Low Conductivity Plasma Sprayed Thermal Barrier Coating Using Hollow PSZ Spheres: Correlation Between Thermophysical Properties and Microstructure, *Surf. Coat. Technol.*, 2008, **202**, p 1994-2001
26. H. Guo, S. Kuroda, and H. Murakami, Microstructures and Properties of Plasma-Sprayed Segmented Thermal Barrier Coatings, *J. Am. Ceram. Soc.*, 2006, **89**, p 1432-1439